Noncontact broadband all-optical photoacoustic microscopy based on a low-coherence interferometer

Zhongjiang Chen, Sihua Yang, Yi Wang, and Da Xing

Citation: Applied Physics Letters **106**, 043701 (2015); doi: 10.1063/1.4906748
View online: http://dx.doi.org/10.1063/1.4906748
View Table of Contents: http://scitation.aip.org/content/aip/journal/apl/106/4?ver=pdfcov
Published by the AIP Publishing

Noncontact broadband all-optical photoacoustic microscopy based on a low-coherence interferometer

Zhongjiang Chen,[1] Sihua Yang,[1] Yi Wang,[2] and Da Xing[1,a)]
[1]*MOE Key Laboratory of Laser Life Science and Institute of Laser Life Science, College of Biophotonics, South China Normal University, Guangzhou 510631, China*
[2]*School of Control Engineering, Northeastern University at Qinhuangdao, Qinhuangdao 066004, China*

(Received 20 October 2014; accepted 14 January 2015; published online 26 January 2015)

We developed and fabricated a noncontact broadband all-optical photoacoustic microscopy (BD-AO-PAM) with a microchip laser and an all-fiber low coherence interferometer. Currently, the available detection bandwidth of the BD-AO-PAM is 67 MHz, and the lateral resolution measured by carbon fibers reaches 11 μm. Furthermore, the imaging capability of the BD-AO-PAM was testified by imaging hairs embedded in scattering gel and *in vivo* blood vessels of a mouse ear. The experimental results demonstrate that the BD-AO-PAM can image the tissues with high spatial resolution *in vivo*, which can be used as portable noncontact PAM for biomedical applications. © *2015 AIP Publishing LLC*. [http://dx.doi.org/10.1063/1.4906748]

Photoacoustic microscopy (PAM) is a hybrid high-resolution and high-contrast noninvasive imaging modality that images optical absorption contrast based on the photoacoustic (PA) effect.[1] PAM has been applied in subcutaneous microvasculature imaging, brain functional imaging, and early detection of tumors.[2–4] Besides, PAM has been used to monitor the blood oxygenation of vessels with high sensitivity and high specificity.[2,5] At present, almost all of the PAMs were still using the ultrasound transducer to detect the PA signals in contact fashion. Owing to the strong attenuation of ultrasound waves in air, the coupling media, such as water or ultrasound gel, has to be added between the sample and ultrasound transducer, which limits the biomedical application of PAM in ophthalmology and surgical navigation. Optical detection of ultrasound is a promising ultrasound detection modality, which can provide high detection sensitivity of ultrasound[6] and broadband width.[7] Meanwhile, the optical detection method can detect the ultrasound signal in noncontact fashion.[6] Therefore, compared with traditional PAM, PAM based on optical detection method has the potential to detect PA signal with high axial resolution and noncontact fashion. Because of the noncontact character of PAM based on optical detection method, it could be conveniently used in many special applications such as the disease diagnosis in ophthalmology and imaging of the affected area in surgical operation.

In past years, more and more optical methods have been presented by using coherent detection approach to measure the vibration velocity and displacement of object surface[6,8–11] or by using polymer-film-based Fabry-Perot interferometer to sense the pressure waves.[12,13] Recent methods employed a time domain optical coherence tomography (OCT)[14] and an intrasweep phase-sensitive OCT[15] for PA signal detection. But these methods could only provide bandwidth-limited ultrasound detection as well as the PZT ceramic transducer. Moreover, the former method was working in the homodyne mode and had to passively detect the ambient vibrations to obtain the highest sensitivity detecting point, which seriously limited the imaging speed and stability of the system. In this letter, we report a noncontact broadband all-optical photoacoustic microscopy (BD-AO-PAM) fabricated with microchip laser and all-fiber low coherence interferometer. In the system, a piezoelectric actuator was added into the reference arm of the low coherence interferometer and generated fast and regular vibrations which can improve the imaging speed and provide stable detecting point. Three dimension (3D) imaging of phantoms and the microvasculature of mouse ear *in vivo* demonstrate that the BD-AO-PAM achieved improvement in the imaging speed, imaging quality, and spatial resolution.

The ultrasound detection process of the noncontact BD-AO-PAM is based on an all-fiber low coherence interferometer, which resolves the phase difference between reference and sample arm along time, giving access to rapid small path length changes such as interface displacement due to a transient PA wave. The intensity $I(t)$ of the low coherence interferometer from the reflective sample surface in the sample arm is given by

$$I(t) \propto \cos(\varphi(t)) = \cos\left(\varphi_0(t) + \varphi_{PA}(t)\right) = \cos\left(\frac{2\pi}{\lambda_0}\left(\Delta z_0(t) + \Delta z_{PA}(t)\right)\right), \quad (1)$$

where $\Delta z_0(t)$ is the optical path difference between reference and sample arm when the PA excitation laser is off, $\Delta z_{PA}(t)$ is the PA pressure-induced surface displacement that allows us to reconstruct the distribution of absorbing sample constituents, and λ_0 is the center wavelength of the detection laser. In order to accurately extract the PA signal from the coherence signal, the system has to be working in homodyne mode, i.e., when $\varphi_0(t) = k\pi \pm \pi/2$, the system has the greatest detection sensitivity for acoustic wave. Generally, $\Delta z_0(t)$ is within the coherence length of the light source, but the ambient vibrations often cause an additional optical path length change, which sometimes can be more than what is expected to detect and resulting in a fluctuating sensitivity for the

a)Author to whom correspondence should be addressed. Electronic mail: xingda@scnu.edu.cn. Tel.:+86-20-85210089. Fax: +86-20-85216052.

system. To address the problem of ambient vibrations, a piezoelectric actuator drove the reference mirror and generated the vibrations which would be faster and more regular than ambient vibrations. So the changes of the additional optical path length would become more regular and faster. And the highest sensitivity points can be easily locked. In doing so, the imaging speed and quality can be improved.

The schematic of the experimental setup is shown in Fig. 1(a). The all-fiber low coherence interferometer consists of a superluminescent diode with a central wavelength of 1310 nm and a spectral bandwidth of 45 nm, an optical circulator, and a 2×2 fiber coupler. A microchip laser (HLX-I-F005, Horus Laser) at 532 nm was used to excite PA signals in the sample. The pulse width of the excitation laser was ~10 ns. To improve the imaging speed and the stability of the system, the piezoelectric actuator was used to drive the reference mirror and generate fast and regular additional vibrations. Because the highest sensitivity of the low coherence interferometer to the vibration is at the point where the optical path length equals to $k\pi \pm \pi/2$, i.e., the output of the photodetector (PDB420C, Thorlabs, USA) is crossing zero, the excitation laser trigger was locked at the zero point by the control card (PCI-1716, Advantech). A trigger signal from the microchip laser was sent to the data acquisition card (NI5124, National Instruments) simultaneously for sampling the PA signals. The timing diagrams triggering the signals acquisition were shown in Fig. 1(b). Fig. 1(c) shows the PA signal obtained from a black tape. To further improve the detection sensitivity of the system, the imaged area of the sample was covered with a thin layer of mineral oil.

The detection bandwidth of the noncontact BD-AO-PAM was measured by detecting the PA signal from the red ink film plated on a transparent thin ployethylene film. The PA signal (no averaging) of the red ink film is shown in the inset of Fig. 2(a). The response spectra of the PA signal is shown in Fig. 2(a), and the −6 dB bandwidth is 67 MHz, which is close to the bandwidth of photodetector (75 MHz). According to the formula: $R_A = 0.88 \bullet V_s/\Delta f$,[16] the axial resolution of the noncontact BD-AO-PAM system is estimated to be 19.7 μm. Fig. 2(b) is the B-scan image in the x-z plane of the red ink film, the full width half magnitude (FWHM) of the profile along z direction is ~20.6 μm, which matches well with theoretical resolution. The results demonstrate that the BD-AO-PAM can provide detection bandwidth of up to 67 MHz. At present, the detection bandwidth of the BD-AO-PAM is limited by the photodetector, employing wider bandwidth photodetector and shorter laser pulse could further improve the detection bandwidth of the BD-AO-PAM.

To quantify the lateral resolution of the noncontact BD-AO-PAM, we imaged two ~6 μm diameter crossed carbon fibers using a scanning step of 3 μm at rate of 40 Hz, and each step averaged 10 times. Fig. 3(a) shows a maximum amplitude projection (MAP) image of the two carbon fibers. In this report, all MAP images were formed by projecting the maximum PA amplitudes along the z axis to the x-y plane. Fig. 3(b) shows the profile of the vertical fiber along x axis, demonstrating that the lateral resolution of our system is at least as fine as 11 μm. The signal-to-noise ratio (SNR), measured from Fig. 3(a), is as high as 19 dB.

We next verified whether the noncontact BD-AO-PAM is capable of imaging the absorption targets within the scattering phantom. To make the phantom, we used four hairs embedded within a scattering gel at depths approximately between 0 and 1 mm. The scattering gel was made of agar mixed with 1% Intralipid, which gave a scattering background similar to typical highly scattering tissue. Fig. 4(a) shows a MAP image of the phantom, and the edge of the hairs is distinct. The depth of the hairs in the scattering gel, z, was extracted using the delay time of the PA amplitude, as shown in Fig. 4(b). The hairs were clearly distributed from 0 to 1 mm in the scattering gel. Meanwhile, the noncontact BD-AO-PAM has 3D imaging capability, the result is shown

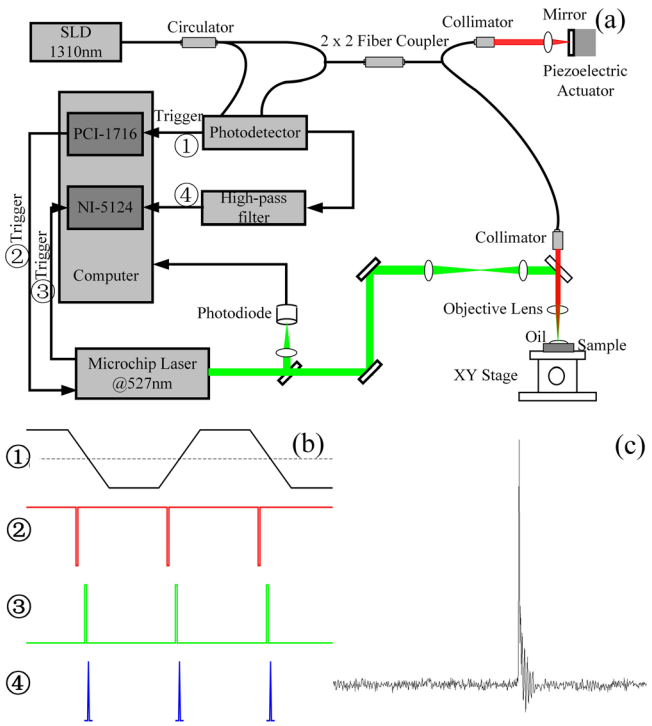

FIG. 1. Schematics and images those describe the experimental setup and its signals acquisition. (a) Schematic of the experimental setup. (b) Timing diagrams for triggering the signals acquisition shown in (a). (c) A PA signal detected from a black tape sample.

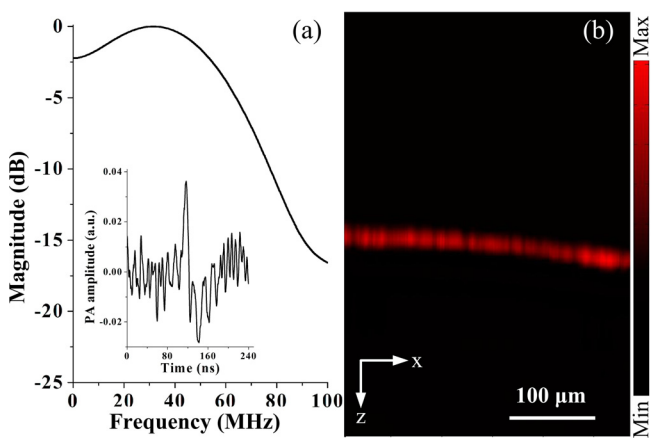

FIG. 2. Detection bandwidth of the noncontact BD-AO-PAM. (a) Spectrum of the PA signal. Inset: the PA signal of red ink film plated on a transparent thin ployethylene film detected by the noncontact BD-AO-PAM. (b) B-scan image in the x-z plane of the red ink film. The total time for obtaining the PA image is 5 s.

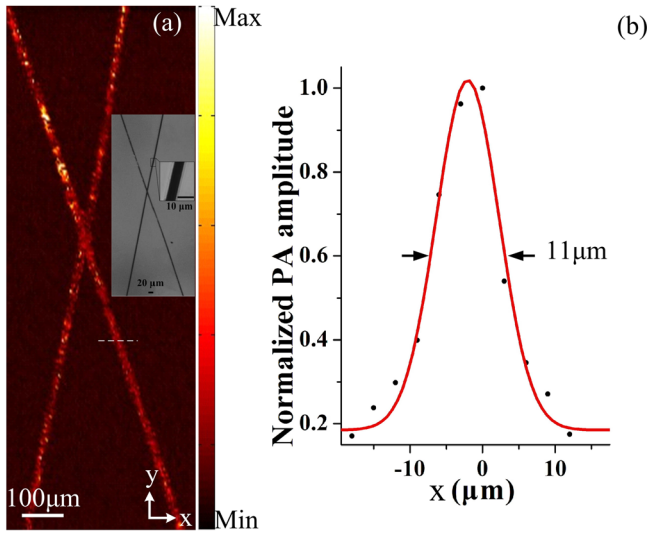

FIG. 3. Lateral resolution of the noncontact BD-AO-PAM. (a) PA image of two crossed 6 μm diameter carbon fibers. The total time for obtaining the PA image is 18.3 min. (b) Distribution of the PA amplitude (dots) along the dashed line in (a). The solid line is a Gaussian fitted curve. Inset: microscopic photograph of the carbon fibers sample.

in Fig. 4(c); the spatial morphology of the hairs is clearly displayed.

To further demonstrate the ability of the noncontact BD-AO-PAM, we used it to image blood vessel of a BALB/c mouse ear *in vivo*. The hair was removed from the ear with commercial hair remover (Payven Depilatory China). Sodium pentobarbital (40 mg/kg; supplemental, 10 mg/kg/h) was administered to keep the mouse motionless during the experiment. All experimental animal procedures were carried out in accordance with the guidelines of the South China Normal University. The laser fluence incident on the skin surface was controlled below 12 mJ/cm^2 in the experiment.

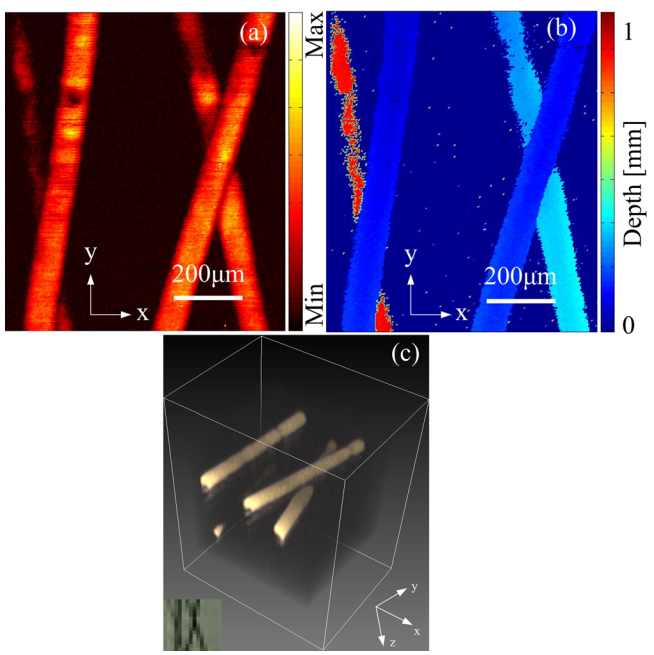

FIG. 4. Photoacoustic image of scattering phantom: (a) Photoacoustic MAP image of the four hairs. The total time for obtaining the PA image is 16.7 min. (b) Depth map of the scattering phantom. (c) Snapshot of a 3D animation showing the four hairs in (a). Inset: photograph of the imaging area.

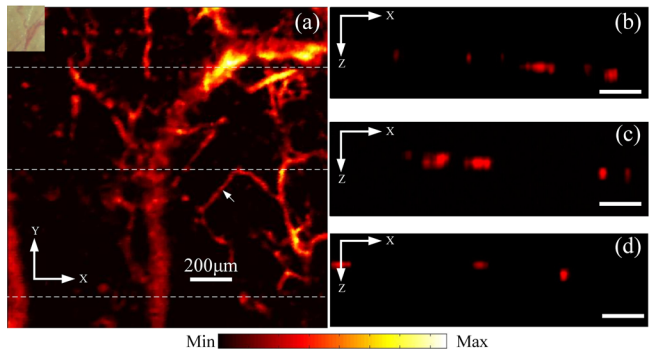

FIG. 5. *In vivo* photoacoustic image of microvasculature of a mouse ear. (a) Photoacoustic MAP image of the microvasculature of a mouse ear. The total time for obtaining the PA image is 16.7 min. Inset: photograph of the imaging area. (b)–(d) B-scan image of microvasculature corresponding to the three white dotted line in (a).

Fig. 5(a) shows the results about microvasculature of mouse ear acquired from an area of 1.6 × 1.6 mm^2 (200 × 200 pixels). The diameter of the blood vessel pointed by the white arrow in the figure is about 12 μm, and the SNR is as high as 24 dB. Figs. 5(b)–5(d) show the B-scan image of blood vessel corresponding to the three white dotted line in (a), and the different size scales of blood vessel along z axis can be clearly distinguished. The results suggest that the noncontact BD-AO-PAM has the capacity to image the microvasculature with high spatial resolution *in vivo*.

All above experimental results show that the PA images of mimic phantoms and biological tissues are reconstructed with high spatial resolution through the noncontact BD-AO-PAM system, which can contribute to promoting the application of PAM. The noncontact BD-AO-PAM uses an all-fiber low coherence interferometer to detect PA signals, and it can be conveniently integrated with OCT and fluorescence imaging to form a multimode imaging system. A multimode imaging system can simultaneously provide more comprehensive anatomical and functional information of biological tissues: This is our next work.

In summary, a noncontact BD-AO-PAM system, consisting of a microchip laser and an all-fiber low coherence interferometer, was developed. The system provided broad detection bandwidth and high imaging resolution, which realized lifelike microvascular imaging on animal model *in vivo*. More importantly, the all-optical character and noncontact fashion of the system makes it easy to integrate a portable system and should be valuable for biomedical applications.

This research was supported by the National Basic Research Program of China (Nos. 2011CB910402 and 2010CB732602), the National Natural Science Foundation of China (Nos. 61331001, 61275214, 61361160414, 81127004, 11104087, and 11304103), the Specialized Research Fund for the Doctoral Program of Higher Education (No. 20114407120001), and the Guangdong Natural Science Foundation (Nos. S2013020012646 and S2013040016419).

[1]L. V. Wang, Nat. Photonics **3**, 503 (2009).
[2]S. A. Ermilov, T. Khamapirad, A. Conjusteau, M. H. Leonard, R. Lacewell, K. Mehta, T. Miller, and A. A. Oraevsky, J. Biomed. Opt. **14**, 024007 (2009).
[3]H. F. Zhang, K. Maslov, M. Sivaramakrishnan, G. Stoica, and L. V. Wang, Appl. Phys. Lett. **90**, 053901 (2007).

[4]S. H. Yang, D. Xing, Q. Zhou, L. Z. Xiang, and Y. Q. Lao, Med. Phys. **34**, 3294 (2007).
[5]Z. J. Chen, S. H. Yang, and D. Xing, Opt. Lett. **37**, 3414 (2012).
[6]G. Rousseau, A. Blouin, and J. Monchalin, Biomed. Opt. Express **3**, 16 (2012).
[7]Y. Hou, J. S. Kim, S. Ashkenazi, S. W. Huang, L. J. Guo, and M. O'Donnell, Appl. Phys. Lett. **91**, 073507 (2007).
[8]T. Berer, A. Hochreiner, S. Zamiri, and P. Burgholzer, Opt. Lett. **35**, 4151 (2010).
[9]B. F. Pouet, R. K. Ing, S. Krishnaswamy, and D. Royer, Appl. Phys. Lett. **69**, 3782 (1996).
[10]M. Paul, B. Betz, and W. Arnold, Appl. Phys. Lett. **50**, 1569 (1987).
[11]S. A. Carp, A. Guerra, S. Q. Duque, and V. Venugopalan, Appl. Phys. Lett. **85**, 5772 (2004).
[12]E. Zhang, J. Laufer, and P. Beard, Appl. Opt. **47**, 561 (2008).
[13]G. Paltauf, R. Nuster, M. Haltmeier, and P. Burgholzer, Appl. Opt. **46**, 3352 (2007).
[14]Y. Wang, C. H. Li, and R. K. K. Wang, Opt. Lett. **36**, 3975 (2011).
[15]C. Blatter, B. Grajciar, P. Zou, W. Wieser, A. J. Verhoef, R. Huber, and R. A. Leitgeb, Opt. Lett. **37**, 4368 (2012).
[16]L. V. Wang and S. Hu, Science **335**, 1458 (2012).